Computer Physics Communications 288 (2023) 108729

Contents lists available at ScienceDirect

Computer Physics Communications

journal homepage: www.elsevier.com/locate/cpc

Z'-explorer 2.0: Reconnoitering the dark matter landscape ☆,☆☆

Víctor Martín Lozano [a], Rosa María Sandá Seoane [b], Jose Zurita [c,*]

[a] Deutsches Elektronen-Synchrotron DESY, Notkestr. 85, 22607 Hamburg, Germany
[b] International Center for Advanced Studies (ICAS), UNSAM, Campus Miguelete, 25 de Mayo y Francia, (1650) Buenos Aires, Argentina
[c] Instituto de Física Corpuscular, CSIC-Universitat de València, E-46980 Paterna, Valencia, Spain

ARTICLE INFO

Article history:
Received 4 October 2021
Received in revised form 7 February 2023
Accepted 16 March 2023
Available online 22 March 2023

Keywords:
LHC
New physics
Exclusion limits
Dark matter

ABSTRACT

We introduce version 2.0 of Z'-explorer, a software tool that provides a simple, fast, and user-friendly test of models with an extra $U(1)$ gauge boson (Z') against experimental LHC results. The main novelty of the second version is the inclusion of missing energy searches, as the first version only included final states into SM particles. Hence Z'-explorer 2.0 is able to test dark matter models where the Z' acts as an s-channel mediator between the Standard Model and the dark sector, a widespread benchmark employed by the ATLAS and CMS experimental collaborations. To this end, we perform here the first public reinterpretation of the most recent ATLAS mono-jet search with 139 fb^{-1}. In addition, the corresponding searches in the visible final states have also been updated. We illustrate the power of our code by re-obtaining public plots and also showing novel results. In particular, we study the cases where the Z' couples strongly to top quarks (top-philic), where dark matter couples with a mixture of vector and axial-vector couplings, and also perform a scan in the parameter space of a string inspired Stückelberg model. Z'-explorer 2.0 is publicly available on GitHub.

Program summary

Program Title: Z'-explorer 2.0
CPC Library link to program files: https://doi.org/10.17632/k7tdp8kwgf.2
Developer's repository link: https://github.com/ro-sanda/Z--explorer-2.0
Licensing provisions: GPLv3
Programming language: C++ and bash
Nature of problem: New SM neutral gauge bosons, Z', are ubiquitously present in models of New Physics. In order to confront these models versus a large and ever-growing library of LHC searches, Z'-explorer 1.0 had already included all final states including Standard Model particles. Notably, the previous version of this tool lacked the so-called *invisible* final states manifested as a momentum imbalance in the transverse plane ("missing energy"). These searches help to probe mediators into a dark sector, where a dark matter candidate resides.
Solution method: Z'-explorer encodes the production cross sections for Z' bosons at the LHC as a function of their mass, allowing for a fast evaluation of the exclusion limits. This version of Z'-explorer includes a careful validation of the latest search with one energetic jet (mono-jet) performed by the ATLAS collaboration. Hence one can now test if a given point in parameter space is excluded by both visible and invisible searches. The modular structure of the code has been kept, which allows for potential additions (low-energy constraints, flavor, extrapolation to future colliders).

☆ The review of this paper was arranged by Prof. Z. Was.
☆☆ This paper and its associated computer program are available via the Computer Physics Communications homepage on ScienceDirect (http://www.sciencedirect.com/science/journal/00104655).

* Corresponding author.
E-mail addresses: victor.lozano@desy.de (V. Martín Lozano), rsanda@unsam.edu.ar (R.M. Sandá Seoane), jzurita@ific.uv.es (J. Zurita).

https://doi.org/10.1016/j.cpc.2023.108729

1. Introduction

Modern model-building requires confronting the parameter space (masses, couplings) of a New Physics model against a large and ever-growing variety of experimental constraints. The reinterpretation of LHC searches can then range from trivial to highly-involved to (almost) impossible. The difficulty of the task can depend on several factors, including the implicit and explicit assumptions of a given study, the degree of model independence, and the public availability of the necessary information to reproduce the reported bounds outside of the specific collaboration (e.g. experimental efficiencies). A fruitful dialogue between the phenomenological and experimental communities is already ongoing [1] which has considerably helped the public reinterpretation effort.

We can classify the re-interpretation codes into two broad categories. First and foremost, the *general* codes provide a framework where any LHC study can be implemented, and those results applied to arbitrary models, e.g. CheckMATE [2,3], MadAnalysis5 [4,5] and GAMBIT [6]. This flexibility on the model independence comes with the price of requiring the generation of a large number of Monte Carlo events in order to confront a single point in parameter space with the experimental data. The second category, *dedicated* codes, narrows the applicability by focusing on a specific model framework (e.g. HiggsBounds [7,8] and HiggsSignals [9] for extended scalar sectors, or SModelS [10] and Fastlim [11] for simplified models), which allows to bypass the CPU-time consuming event generation and thus allow a fast exploration of the parameter space. In the latter category belongs our tool, Z'-explorer [12] which focuses on models where the SM is augmented with a new $U(1)$ gauge boson, dubbed Z'.

Z'-models are widely used in a variety of contexts, see e.g. [13,14] for a review. Of our particular interest is a Z' boson acting as an s-channel mediator to the dark sector [15,16]. The existence of the mono-X process $pp \to Z'X \to \chi\chi X$, where $X = j, \gamma, Z, W, \ldots$ is a Standard Model (SM) particle that must be present for the event to be recorded on tape ("triggered"), requires that the Z' couples to both the Standard Model and the dark matter candidate χ. This provides a robust foundation to the existing mediator search programme at the LHC, encompassing both *visible* (i.e. Standard Model) and *invisible* (dark sector) final states. Having a fast and flexible tool for the simultaneous reinterpretation of the broad palette of experimental searches is a desirable addition to the model builder's toolkit. The first step in that direction was done in Z'-explorer 1.0, where the whole suite of visible final states was implemented [12], requiring as user input only the Z' mass and its coupling to SM particles, which avoids the need for event generation.

In this article, we extend the capabilities of Z' explorer to further include searches with missing energy. To that effect, we perform (to the best of our knowledge) the first public reinterpretation and validation of the ATLAS mono-jet study with 139 fb^{-1} of total integrated luminosity [17], which provides the most stringent constraints from the whole set of mono-X searches when X comes from initial state radiation [18]. When compared to ZPEED [19] (which included all Z' decays into di-jet and di-lepton channels), Z'-explorer additionally includes the WW and Zh channels (from version 1.0) and the missing energy studies described in this article (version 2.0).

Our code goes beyond the public results presented by ATLAS in two directions. First and foremost, we allow for arbitrary couplings to every SM fermion. The oversimplifying assumption of having one single common quark coupling g_q and/or a single lepton coupling g_l can be dropped, revealing an interesting interplay between the visible and invisible sectors. We note that in this case, since Z'-explorer does yet not include constraints from flavor physics (which can nonetheless be easily obtained from e.g. `flavio` [20]), the user must take them separately into account. Second, we consider a general coupling structure for the $Z' - \chi - \chi$ vertex, going beyond the two benchmark setups commonly used by the experimental collaboration: the vector and axial-vector scenarios. Our results are implemented in Z'-explorer 2.0, which is publicly available on GitHub [21]. Since Z'-explorer does not require simulating events, it is appropriate for a thorough scanning of the parameter space when compared to general re-interpretation codes.

The current article is structured as follows. In section 2 we review the fundamentals of Z' models, presenting the parametrization used within Z'-explorer, which coincides with the one adopted by the Dark Matter Working Group (DMWG) [16].[1] In section 3 we present the validation of the ATLAS mono-jet study [17]. We exemplify the impact of Z'-explorer by applying it to a series of examples in section 4, and we reserve section 5 for our conclusions. Technical details regarding the software implementation are left for Appendix A.

2. Z' models: theoretical framework

In this section, we present a summary of the theoretical framework (for details we refer the reader to [15]) and describe in a nutshell the main features of the dark sector implementation in Z'-explorer 2.0, while the technical details are presented in Appendix A.

We augment the SM with a new $U(1)$ gauge boson Z' and a SM singlet Dirac fermion χ. The latter is our dark matter candidate, rendered stable by a discrete $\mathbf{Z}_2$ symmetry, as customary in dark matter models. The SM fermions f and the dark matter χ have arbitrary left- and right-handed couplings, $g^{L,R}_{f,\chi}$ to the Z' mediator. The relevant Lagrangian then reads

$$\mathcal{L} \supset Z'_\mu \left[\sum_f \left(g_{f_L} \bar{f}_L \gamma^\mu f_L + g_{f_R} \bar{f}_R \gamma^\mu f_R \right) + g_{\chi_L} \bar{\chi}_L \gamma^\mu \chi_L + g_{\chi_R} \bar{\chi}_R \gamma^\mu \chi_R \right], \tag{1}$$

where the index f runs over all the SM fermions (for the treatment of neutrinos see Appendix A). This Lagrangian coincides with that adopted by the ATLAS and CMS collaborations [15] when all the leptonic couplings are set to zero, and when the Z' has either vector ($g_{f_L} = g_{f_R}$) or axial-vector ($g_{f_L} = -g_{f_R}$) couplings to the SM quarks and to the dark matter χ. While it has been shown that the different couplings in equation (1) must obey non-trivial constraints among them if unitarity and gauge invariance are imposed [22,23], we consider this framework a minimal parametrization of richer models, that could feature more than one mediator and/or new dark states beyond Z' and χ. Hence each left- and right-handed (or axial and vector) coupling is treated as a free parameter by Z'-explorer. We also contemplate the possibility of Z' decays into new, non-SM states (other than $\chi\chi$) parametrized by an unknown decay width Γ_{xx}. In comparison with Z'-explorer 1.0, the new parameters the user must input are the dark matter mass m_χ and the dark matter couplings to the Z', $g_{\chi_{L,R}}$.

A foundational ingredient of Z'-explorer's philosophy is to employ the *expected* limits instead of the observed ones. This is an approximation that holds as long as no large fluctuations in the data are present. The rationale behind it is to be able to disentangle the

[1] Except that the DMWG employs the vector (V) - axial-vector (A) basis for the couplings, instead of the left-right used in Z'-explorer.

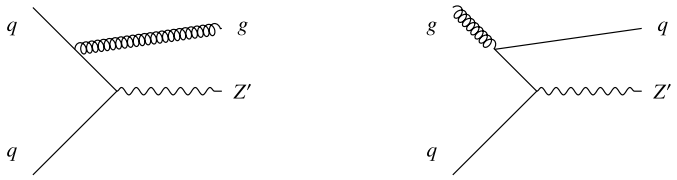

Fig. 1. Feynman diagrams of the Z' production with a radiated jet from the initial state. This process could be initiated either by a pair of quarks radiating a gluon (left) or a pair gluon quark where a quark is radiated (right).

experimental sensitivity of a given channel from these fluctuations. In its current form, Z'-explorer would not be appropriate in a discovery (or large significant fluctuation) scenario. We emphasize, again, that the goal of Z'-explorer is to set exclusion bounds on the parameter space given by equation (1). Hence through this work, all limits and background events reported correspond to the *expected* case, unless noted otherwise.[2]

A key constituent of Z'-explorer is the narrow-width approximation (NWA), which allows factorizing the LHC processes involving Z' as a *production cross section* times a corresponding branching ratio in a given channel. It is then important to check if the approximation is fulfilled. The calculation of the Z' partial width at leading order (LO) is straightforward and full expressions are presented in Ref. [15]. In the limit where $m_{f,\chi} \lesssim M_{Z'}$ the Z' width is independent of the left- and right-handed coupling structure, reading

$$\frac{\Gamma_{Z'}}{M_{Z'}} = \frac{1}{12\pi}\left(g_\chi^2 + \sum_f N_C g_f^2\right), \tag{2}$$

where N_C is the number of colors of each SM fermion f: 3 for quarks and 1 for charged leptons. Z'-explorer does not stop the execution of the code, but prints a warning in the output if the width-to-mass ratio of equation (2) is larger than 5%. For a leptophobic Z' with a single g_q coupling being equal to (4 times smaller than) g_χ, this 5% threshold is reached for $g_q = 0.35(0.25)$, which sets a ballpark value for these couplings. We note that even if the width is small, interference effects can be important if the lepton decay rates are appreciable, as discussed in reference [19]. This work introduced the public code ZPEED. In comparison with Z'-explorer, ZPEED outputs the likelihoods for a given point in parameter space while including the relevant interference effects, but it does not include SM final states with gauge bosons and scalars (W^+W^-, Zh) and neither does include invisible decays.

The model described by equation (1) has been implemented in the Universal Feynman Output [24] (UFO) format in reference [25]. Along this work, we will employ `MadGraph5_aMC@NLO` [26] for event generation at the parton level, `Pythia 8` [27] for showering and hadronization, and `Delphes 3.4.2` [28] for detector simulation, using the default ATLAS card. We will work at leading-order (LO) accuracy in the strong coupling, which is justified since next-to-leading order QCD effects have been found to be quite mild [29].

A series of sanity checks have been performed with the UFO model. On one hand, we have verified the validity of the partial widths expressions by numerically comparing the evaluation of the analytic expressions from [15] with the output of MadWidth [30]. On the other hand, we have studied several kinematical distributions (in particular missing transverse energy, and the leading jet momenta and the jet pseudorapidities) to verify that, as expected, the shape of these distributions (which are those employed by ATLAS and CMS) depends only upon $M_{Z'}$ and m_χ, while being independent of all couplings. This is a crucial assumption upon which Z'-explorer relies.

The quark couplings obviously enter in the production cross-section for the $pp \to Z'j$ process. The two main processes for $pp \to Z'j$ are shown in Fig. 1, in the first one, a pair of quarks annihilate to produce a Z' while a gluon is radiated from one of them (left diagram from Fig. 1). The other process is initiated by a gluon and a quark. The gluon splits into two quarks, one of them annihilates with the other initial quark to give a Z' while the other is radiated. We have also verified that the different quark contributions from the initial state do not interfere with each other, namely that

$$\sigma(pp \to Z'j) = \sum_{q_i} g_{q_i}^2 \left[\sigma(q_i\bar{q}_i \to Z'g) + \sigma(q_i g \to Z'q_i) + \sigma(\bar{q}_i g \to Z'\bar{q}_i)\right], \tag{3}$$

holds. We note that the different cross-sections σ in the square brackets are *not* parton level matrix-elements, but they also include the corresponding convolution with the parton distribution functions (PDF). Here we assume that CP is conserved, hence the difference between $q_i g$ and $\bar{q}g$ initial states is only due to the PDFs.

For the fast evaluation of these production cross-sections, we follow a procedure analogous to the one used in Z'-explorer 1.0. For the visible channels, the relevant process under consideration is $q_i\bar{q}_i \to Z'$. Due to the trivial scaling with the g_q couplings and the lack of interference among the different channels, it is enough to make a fine scan of $\sigma(q_i\bar{q}_i \to Z')$ in the 1-dimensional parameter space given by $M_{Z'}$. Here the task is slightly more complicated since now the different cross-sections from equation (3) must be scanned in the two-dimensional mass plane $M_{Z'} - m_\chi$. Nonetheless, this is not an obstacle, and with a fine scan of this mass plane, the cross-section of any given point can be numerically estimated with great accuracy, as described in Appendix A.

One point to be noticed here is that we do not consider here the constraints coming from dark matter. The relic density is a complex function of g_q, g_l, g_χ and the Z' and χ masses. Besides the dependence on many variables, it is also possible that the relic density can suffer modifications if e.g.: it is produced non-thermally, or if the universe follows a non-standard (yet 100% viable) cosmological history that could add additional annihilation (or creation) mechanisms. Furthermore, there are other tools that are available to the public that specifically oriented to test these subjects, such as `MicrOmegas` [31] and `MadDM` [32]. The impact of direct detection for Z'-models have been studied in reference [15] while a scan over the typical allowed and excluded regions for models of dark matter with a Z' mediator performed by ATLAS collaboration can be found in [33].

[2] It is foreseen in future versions of this software to allow the user to choose between the expected (as done here) and observed limit (as done in e.g. `HiggsBounds` [7,8] and `CheckMate` [2,3]).

Table 1
Exclusive (EM0-EM12) signal regions defined in ATLAS monojet search at 13 TeV and 139 fb^{-1}, together with the expected number of background events.

Exclusive	EM0	EM1	EM2	EM3	EM4	EM5	EM6
E_T^{miss} [GeV]	200-250	250-300	300-350	350-400	400-500	500-600	600-700
Predicted	1783000	753000	314000	140100	101600	29200	10000
Exclusive	EM7	EM8	EM9	EM10	EM11	EM12	
E_T^{miss} [GeV]	700-800	800-900	900-1000	1000-1100	1100-1200	> 1200	
Predicted	3870	1640	754	359	182	218	

3. ATLAS search for Z' mediators to the dark sector

In this section, we perform the validation of the ATLAS mono-jet search with 139 fb^{-1} and explain the implementation in Z'-explorer 2.0. We comment on the shortcomings of our validation while making suggestions for the improvement of the reinterpretation material.

There is a large number of mono-X searches conducted by the ATLAS [17,34–37] and CMS collaborations [38–41]. In our Z' setup, with only one mediator and one dark matter particle, the X particle comes exclusively from initial state radiation (ISR) and it has been shown that in the Z' model under consideration in this work, the mono-jet search trumps over all the others mono-X searches [18]. We will then focus on the latest ATLAS mono-jet analysis [17].[3] Nonetheless, for successful validation of this channel, we will also consider an older version of the study, using 36.1 fb^{-1} [42] of total integrated luminosity since each search presents different benchmark points. The latter study had been implemented in the Physics Analysis Database (PAD) of MadAnalysis5 [43], which provided a useful cross-check of our signal cutflows.[4] Nonetheless, due to the modular nature of Z'-explorer, and the goal to keep it as flexible as possible for future updates, we plan to implement the neglected mono-X studies in a future release including more general dark matter sectors. In that case, final state radiation (FSR) also plays an important role and hence there is no "a-priori" predominance of the mono-jet channel.

The ATLAS study with 139 fb^{-1} considers events that passes the $E_T^{miss} > 200$ GeV trigger, and requires the presence of at least one energetic jet j_1 fulfilling $p_{T,j_1} > 250$ GeV and $|\eta| < 2.4$, while up to a maximum of 4 jets with $p_T > 30$ GeV and $|\eta| < 2.8$ are allowed. In all cases, there is a minimum azimuthal distance requirement between each jet and the direction of the transverse missing momentum, $\Delta\phi(jet, \vec{p}_T^{miss}) > 0.4(0.6)$ for $E_T^{miss} > 250$ GeV ($E_T^{miss} \in [200 - 250]$ GeV). To complete the event selection, events with leptons (e, μ, τ) or photons are vetoed.

After this event selection, the analysis is performed using two sets of signal regions: an *inclusive* selection (IM1, IM2, ...) and an *exclusive* one (EM1, EM2, ...). As their names suggest, the inclusive analysis requires E_T^{miss} above a certain threshold value, while the exclusive analysis requires a specific interval. The exclusive signal regions (which are those employed by Z'-explorer), with their E_T^{miss} thresholds, are detailed in Table 1. The previous version of this study uses a similar cutflow, albeit with fewer signal regions, tighter cuts on E_T^{miss} and looser requirements on e, μ and no τ neither photon vetoes. Since the exclusion curves are only derived for the exclusive bins, we will restrict ourselves to the EMi regions. For completeness, we also present in Table 1 the expected (predicted) number of background events in each of them.

For our validation, we turned to the publicly available material. The latest study uses as a benchmark point $M_{Z'} = 2000$ GeV and $m_\chi = 1$ GeV, while the previous version employs $M_{Z'} = 1000$ GeV and $m_\chi = 400$ GeV, and a universal coupling to quarks g_q is set to 0.25, while g_χ is fixed to 1. These two benchmark points represent different kinematic regimes (in the former we can neglect the effect of m_χ while in the other the dark decay is close to the threshold), and hence the combination of both provide crucial information for the proper reinterpretation.

The ATLAS study only presents results for the vector mediator and axial-vector mediator cases. ATLAS provides an official cutflow for one benchmark point (in the 139 fb^{-1} version), and the E_T^{miss} distribution for the signal benchmark and the background. The previous version of this study presented in addition (for the other benchmark point) the leading jet transverse momentum $p_T(j_1)$ distribution, which provides a welcome additional cross-check of the validation procedure.

Regarding the 95% confidence level (CL) exclusions, ATLAS presents the results for the observed upper limits (UL) on the product of the signal cross-section, acceptance, and efficiency using the inclusive selection, and the 95% CL exclusion curves using the exclusive selection. This creates an additional difficulty for the validation, as i) only the *observed* UL are reported, and not the expected ones, ii) the use of different selections between the UL and the exclusion curves prevents the derivation of the exclusion contours from the UL and iii) correlations among the different bins are not reported.

We present in Fig. 2 the missing energy distributions obtained for the axial-vector case by ATLAS, together with the result of our simulations. In the left panel, we present the 36 fb^{-1} study, while in the right panel we present the results for 139 fb^{-1}. In order to match the published distributions, we need to include a global k-factor[5] of 0.80 ± 0.02, whereas the older version (for a different benchmark point and with fewer background events, hence a larger statistical error) required 0.82 ± 0.02.[6] We can then conclude that our event generation pipeline is validated, although as mentioned additional distributions, and potentially additional benchmark points would be a desirable addition, following also the recommendations in Ref. [1]. In passing, we note that we have also investigated here the

[3] While this work was in the final stages of completion, updated monojet results by the CMS collaboration were made public [38]. Their sensitivity to the axial-vector scenario is comparable with the ATLAS result.

[4] We are indebted to Benjamin Fuks for providing us with MadAnalysis5 v.1.9.35.

[5] We employ the lowercase k-factor for the overall normalization required to match the experimental results, namely this is the ratio of the reported events by ATLAS over the predictions of our own Monte Carlo simulation. These k-factors should not be confused with the uppercase K-factor which encapsulates the impact of radiative corrections (which we neglect in this work), as the latter is customarily used in the literature for both QCD and electroweak corrections. The sources of the k-factors are multifold, including the impact of the radiative corrections, the efficiencies of triggers, the object reconstruction algorithms and detector effects. Among them, an important effect is how the energy-momentum measurements of a jet is rescaled from the parton to the reconstructed level, see [44,45] for details.

[6] The uncertainty in these k-factors is obtained by simple error propagation from the statistical uncertainty of our simulated Monte Carlo events and from the ATLAS reported number of events. The latter uncertainty is not reported, hence we estimate it from the statistical uncertainty $\sqrt{n}$.

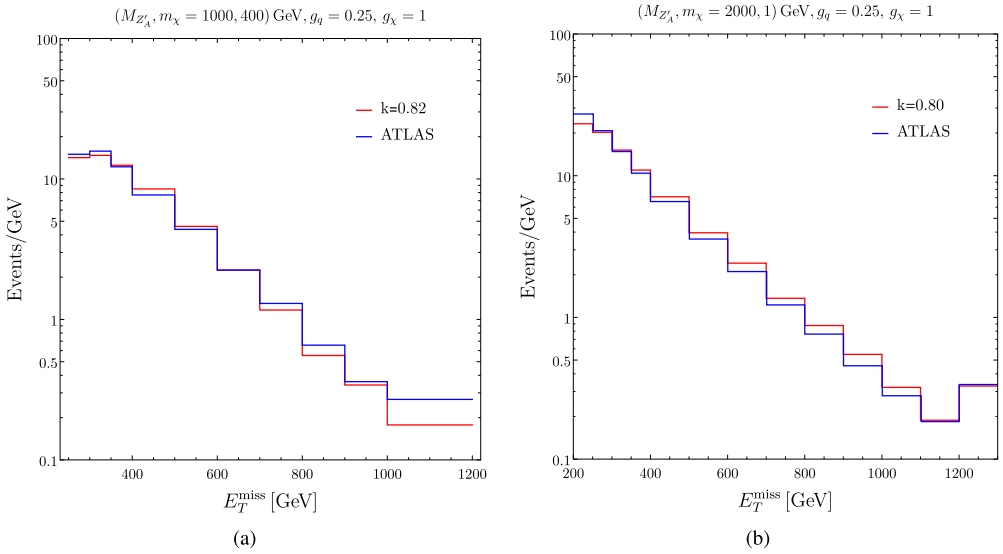

Fig. 2. Missing transverse energy distributions for a signal point with $g_q = 0.25$, $g_\chi = 1$, and (a) $M_{Z'} = 1000$ GeV, $m_\chi = 400$ GeV; (b) $M_{Z'} = 2000$ GeV, $m_\chi = 1$ GeV in the axial-vector mediator scenario. A flat k-factor of 0.82 (0.80) has been applied in the left (right) panel. (For interpretation of the colors in the figure(s), the reader is referred to the web version of this article.)

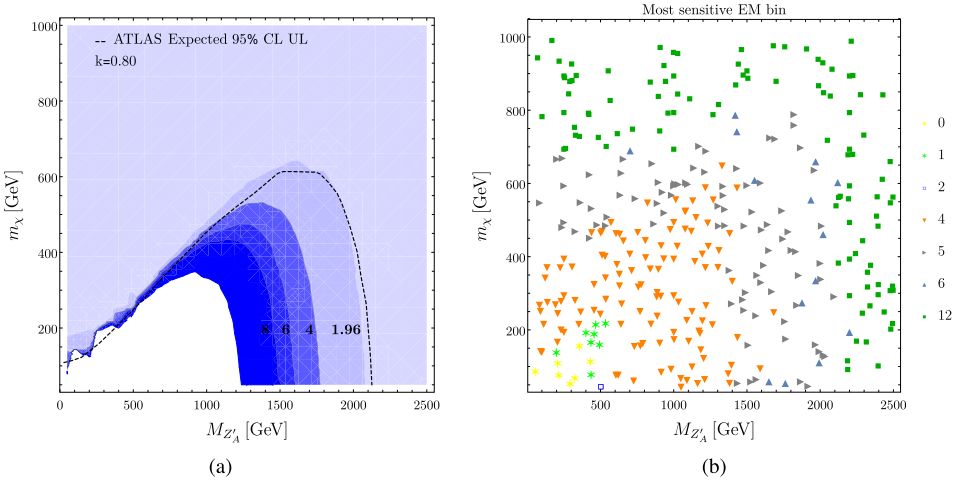

Fig. 3. (left) 95% C.L. exclusion contours for the significance $z = 2, 4, 6, 8$ and the exclusive selection in Table 1, for an axial-vector mediator, with $g_\chi = 1$ and $g_q = 0.25$. (right) Most sensitive exclusive bin for all the reference points considered in the $(M_{Z'}, m_\chi)$ plane, for an axial-vector (b) mediator with $g_\chi = 1$ and $g_q = 0.25$, where the sensitivity is estimated in the Gaussian limit.

impact of jet-matching / merging together with the different options for the dynamical scale choices offered by `MadGraph5_aMC@NLO`. The effect is at the percent level, and as such can be ignored if we take into account that ATLAS reports 10% of uncertainty in the signal modeling and 10% of uncertainty stemming from the parton distribution functions (PDF).

We then proceed to derive the 95% C.L. exclusion contours for the axial mediator model, which we present in the left panel of Fig. 3. We have considered here 366 points in the 2D mass plane. We display the contours where the significance $z = s_i/\sqrt{b_i}$ is 2,4,6 and 8, together with the ATLAS 95% C.L. expected exclusion (dashed black line).[7]

Considering that the latter is derived from a different event selection than the former, the agreement is striking. We also provide, in the right panel of Fig. 3 the most sensitive EM signal region for all of our scanned points. This is an interesting plot for two reasons. First and foremost, it provides important insight on the impact of each signal region and can help to better understand the limits and suggest improvements to the search. Second, this is a relatively simple piece of information to provide, and that would be helpful as now the published table with the 95% UL on the signal rates could be directly employed. For completeness we present the analogues of Fig. 3 for the vector mediator case, in Fig. 4. We see that the situation is completely analogous, except that the excluded regions do not fully due to the difference in cross-sections for each case.

[7] Note that our estimated significance is strictly valid in the limit where $\sqrt{b_i} >> 1$ and $s_i < \sqrt{b_i}$. We have explicitly verified that these two conditions are fulfilled in all the parameter space, given the values of b_i in the signal regions reported in Table 1, and the necessary amount of signal events for a 95% C.L. exclusion.

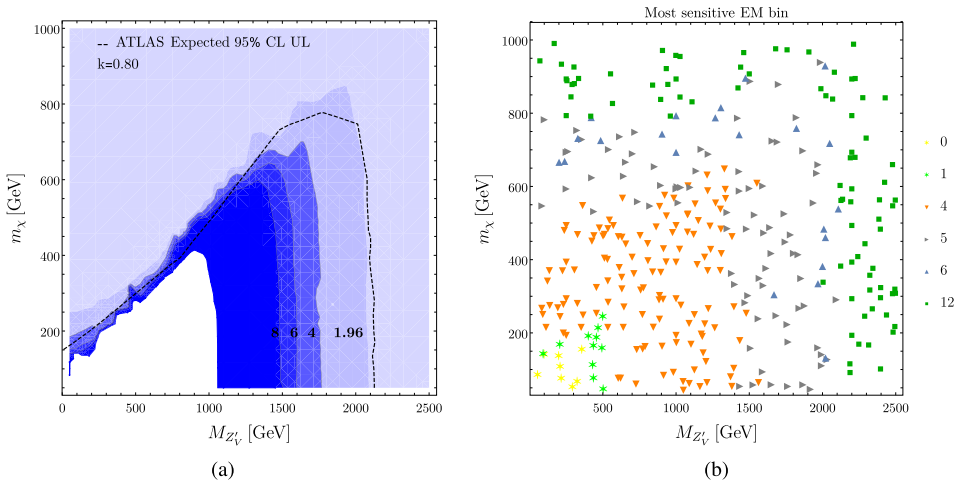

Fig. 4. Same as Fig. 3, for the vector mediator case.

Table 2
Experimental searches at $\sqrt{s} = 13$ TeV included in Z'-explorer 2.0.

Channel	Luminosity	Collaboration	Ref.
jj (dijet)	139 fb^{-1}	ATLAS	[46]
$b\bar{b}$	139 fb^{-1}	ATLAS	[46]
$t\bar{t}$	35.9 fb^{-1}	CMS	[47]
e^+e^-	137 fb^{-1}	CMS	[48]
$\mu^+\mu^-$	140 fb^{-1}	CMS	[48]
$\tau^+\tau^-$	36.1 fb^{-1}	ATLAS	[49]
W^+W^-	36.1	ATLAS	[50]
Zh	35.9 fb^{-1}	CMS	[51]
$\chi\bar{\chi}$ (monojet)	139 fb^{-1}	ATLAS	[17]

From these two figures, we then conclude that the ATLAS mono-jet search, despite lacking some detailed validation material, has been reproduced with an exceptionally good agreement,[8] and hence we will consider the implementation of this study in Z'-explorer 2.0 as validated, and we make the code publicly available on GitHub [21].

4. Numerical results

In this section we present several plots obtained with Z'-explorer 2.0, which serve as an illustration of its capabilities. For each example, we will present the exclusions in the two-dimensional $M_{Z'} - m_\chi$, and we will adopt the following convention to display our results. The most sensitive channel in a given point in the mass plane is indicated by its shape (stars, circles, diamonds, etc). If a given point is allowed (i.e. not excluded) then the shape is shown in a color other than black, while excluded points have a shape in black. The most sensitive channel is determined through the *strength* ($\mathcal{S}$) of the signal of each channel, extracted from the output of Z'-explorer 2.0 (see Appendix A.2 for further details). If for any given channel $\mathcal{S}_i > 1$, the point is experimentally excluded. Conversely, if $\mathcal{S}_i < 1$ for all channels, the point is then allowed, and also the channel with the largest S is expected to be the most sensitive channel for the expected exclusion (or observation) of the given Z'. The channels and their labels we use in order to confront the results of the Z' are: dijet (jj), two b quarks ($b\bar{b}$), two t quarks ($t\bar{t}$), dielectron (e^+e^-), dimuon ($\mu^+\mu^-$), ditau ($\tau^+\tau^-$), di-W boson (W^+W^-), Z plus h bosons (Zh) and monojet ($\chi\chi$) signature. For completion, we display in Table 2 the whole catalog of visible searches in Z'-explorer 2.0. All these experimental searches have been validated in the first version of Z'-explorer [12]. Studies updated after the publication of reference [12] need no additional cross-check since only the upper limits in the 1-dimensional new physics parameter space have been straightforwardly updated.

We will start first working directly on the parametrization of equation (1), where each individual coupling is considered a free parameter. Within this framework, we will restrict ourselves to a few slices of the parameter space, stressing the non-trivial interplay among the different search channels. In the second place, we will consider a complete model, a string inspired Stückelberg portal, where there are non-trivial correlations among the different couplings.

[8] The agreement is less impressive in the whole compressed region, and especially also for small Z' masses. This is totally expected as this regime is quite challenging from an experimental perspective, and the analysis loses sensitivity since the compressed spectrum also implies a softer MET distribution. Here we consider *compressed* the regime where $1 - 2m_\chi/m_{Z'} \lesssim 0.1$, although we stress that the actual cutoff value is arbitrary. Furthermore, there are regions in the large $M_{Z'}$ range where the agreement is in the 10 s of % range.

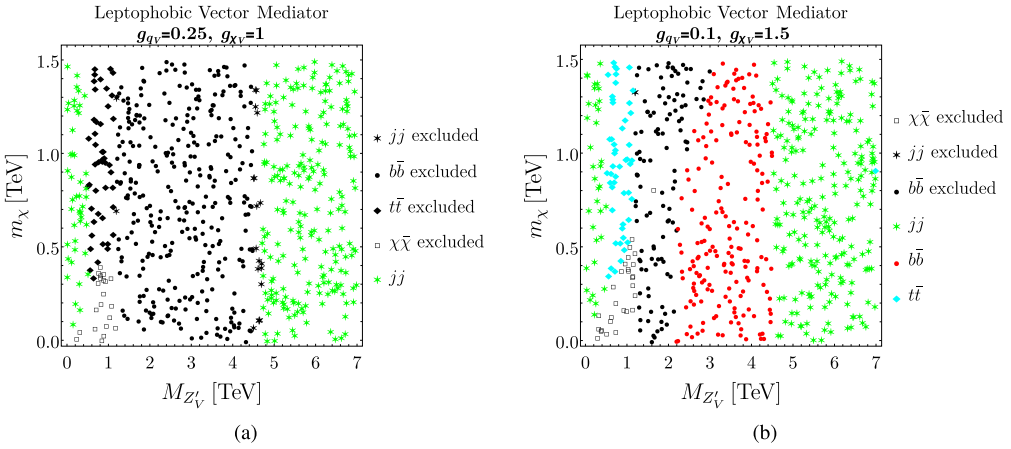

Fig. 5. Excluded parameter space and most sensitive channel for the case where the dark matter couples with vector couplings, for two leptophobic $g_l = 0$ scenarios, fixing $g_q = 0.25$ and $g_\chi = 1$ (left) and $g_\chi = 1.5$ (right). The shape of each point shows the most sensitive channel, while a black (colored) point indicates if it is excluded (allowed).

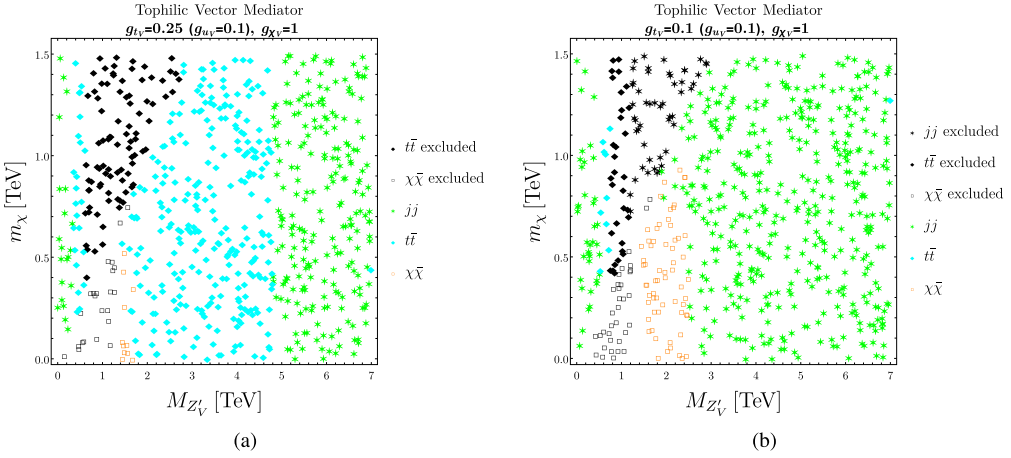

Fig. 6. Excluded parameter space and most sensitive channel for the case where the dark matter couples with vector couplings, for two top-philic scenarios (and also leptophobic), fixing $g_u = 0.25$ and $g_\chi = 1$, with $g_t = 0.25(0.1)$ in the left (right) panel and $g_\chi = 1.5$ (right).

4.1. Simplified model

We start first by examining the benchmark couplings of $g_q = 0.25$, $g_\chi = 1$, $g_l = 0$ used by the ATLAS monojet-study, and for comparison we also include a slightly altered version with $g_\chi = 1.5$. These two *leptophobic* cases are shown in the left and right panel of Fig. 5.

From the figure one clearly sees the impact of the mono-jet search. Clearly, when the dark matter channel is kinematically closed, the situation is relatively simple: depending on the specific mass, a hadronic channel (either jj, $b\bar{b}$ or $t\bar{t}$) provide the strongest constraints. The excluded masses range then from 0.5 to 4.5 TeV approximately, with the upper value being due to a reduction of the production cross-section, while the lower value is because Z'-explorer only included information on the visible channels from 400 GeV. This limitation is due to the fact that for lower masses, the inclusive H_T trigger is less efficient due to the overwhelming QCD multi-jet background.[9] The mono-jet channel is only relevant for the on-shell region, but as soon as it is open it dominates the exclusion, up to a value of $M_{Z'}$ of about 1 (1.5) TeV in the left (right) panel. Comparing the shape of the mono-jet exclusion among both panels, we see that it is relevant for the case where g_χ dominates over g_q.

In second place we consider the case where the Z' decays almost exclusively to the top quark (top-philic Z') while still being leptophobic $g_l = 0$. Note that a non zero g_q for u, c, d, s needs to be added in order to produce the Z' at the LHC. For simplicity and to avoid having to consider FCNC bounds, we set consider all fermions coupling vectorially, and set $g_u = 0.1$, and set $g_\chi = 1$. We present in the left (right) panel of Fig. 6 the different exclusions for a medium (small) g_t couplings: 0.25 (0.1).

As expected, this figure illustrates that when the Z' couples more strongly to tops, the sensitive channels in light di-jet resonance become ineffective, and the mono-jet channel can be the most sensitive one in a large fraction of parameter space. We note that in particular, the mono-jet channel can be the most sensitive up to masses of about 2.5 TeV (obviously having the $Z' \to \chi\chi$ channel open).

For the next example, we drop the assumption of the Z' being leptophobic, and hence consider both vector and axial vector scenarios, with $g_q = 0.1$, $g_\chi = 1$ and $g_l = 0.01(0.1)$ for the vector (axial-vector) case. The results plots are shown in the left and right panel of Fig. 7.

[9] Nonetheless, there are efforts to reduce this threshold and extend the analysis into lower masses, see e.g. [52–54].

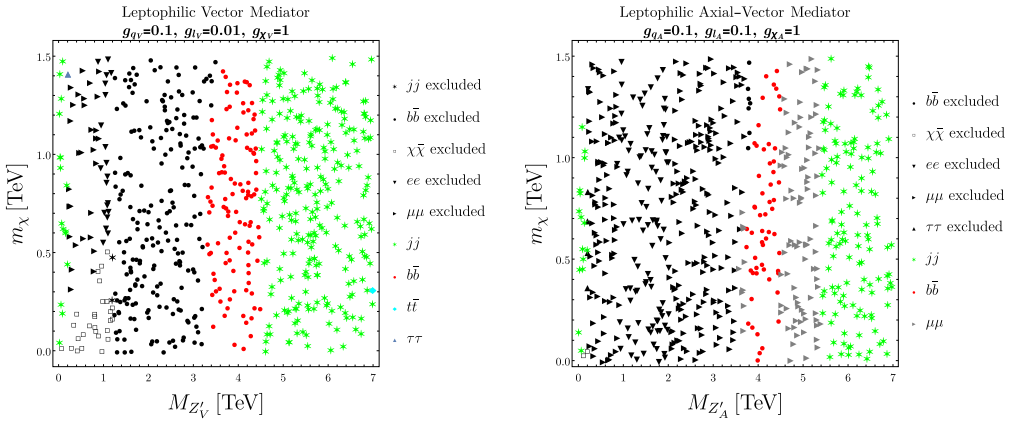

Fig. 7. Same as Fig. 5 and 6, yet allowing for a non-zero coupling to leptons. We set $g_q = 0.1$ and $g_\chi = 1$, and show the results for $g_l = 0.01(0.1)$ in the left (right) panel, for the vector (axial-vector) case.

Table 3
Charge assignment of the SM matter particles under the four $U(1)$ factors of Ref. [57].

Matter field	Q_A	Q_B	Q_C	Q_D	Y
Q_L	1	-1	0	0	1/6
q_L	1	1	0	0	1/6
U_R	-1	0	1	0	-2/3
D_R	-1	0	-1	0	1/3
L	0	-1	0	-1	-1/2
E_R	0	0	-1	1	1
N_R	0	0	1	1	0

From the figure, we clearly see that the lepton channels are very sensitive, and if they are open they can dominate the exclusions. For large enough couplings the mono-jet search is much less sensitive than the di-lepton channels, except for the case where $g_l = 0.01$, where more points have mono-jet as the most sensitive probe.

Next, we examine dropping the assumption that the Z' must be either a vector or an axial-vector. We then consider a generic mixing angle among both possibilities, first for the quarks, and then for the dark matter χ, both in Fig. 8. In each figure we fix the absolute value of $g_\chi = 1$ and $g_q = 0.1$. We fix also one of the couplings in vector type, and for the other coupling, we consider three phases: 30°, 45° and 60° ($\theta = 0°$ corresponds to a pure axial-vector case, and $\theta = 90°$ to a pure vector case). What see in the figures is that the exclusions are rather similar, only presenting small variations. We thus conclude that while one can in principle be sensitive to the phase, in practical terms the variation with the angle is fairly small and can be hard to extract, from a potential signal, the θ phase.[10]

4.2. Stückelberg portal from intersecting D6 branes

Next, we will test the power of the tool Z'-explorer with a complete model that involves more complicated relations among the couplings of the Z'. This particular model consists of a Stückelberg portal that could arise from intersecting D6 branes that were studied in Refs. [58–60]. We will focus on a particular gauge sector given by

$$SU(3)_c \times SU(2)_L \times U(1)_V^A \times U(1)_V^B \times U(1)_V^C \times U(1)_V^D \times U(1)_h^m \times G_h, \tag{4}$$

where the subscript V and h corresponds to visible and hidden sector respectively, $U(1)_h^m$ are the m abelian gauge factors that only couple to the hidden sector while G_h is the semi-simple part of the hidden gauge group. Within the visible sector, there is four abelian gauge factor that couple to visible matter fields. Each of these factors[11] has a charge Q_α under which the SM matter particles are charged. The charges of the SM matter particles in terms of the four visible $U(1)$ are listed in Table 3. In order to have an anomaly-free model the quark sector is split into two assignments, being $Q_L = t_L, b_L$ and $q_L = u_L, c_L, d_L, s_L$. If we have a look at Table 3 we can see that the different charges are related to different physical properties. Q_A is related with baryon number, Q_D with lepton number while Q_B and Q_C are related with the left and right nature of the matter particle.

In order to obtain the gauge group of the SM, a linear combination of the four charges must give rise to the hypercharge.

$$Q^Y = \frac{1}{6}(Q_A - 3Q_C + 3Q_D). \tag{5}$$

[10] With enough signal events, one could construct forward-backward asymmetries [55] or consider a binned study in rapidity [56].

[11] These factors arise from the different overlapping branes that intersect while obtaining the SM from type IIA string theory, this realization is the so-called *Madrid quivers* that is one of the simplest realistic models of intersecting D6 branes [57]. A stack of N branes usually hosts a gauge group $U(N) \cong SU(N) \times U(1)$.

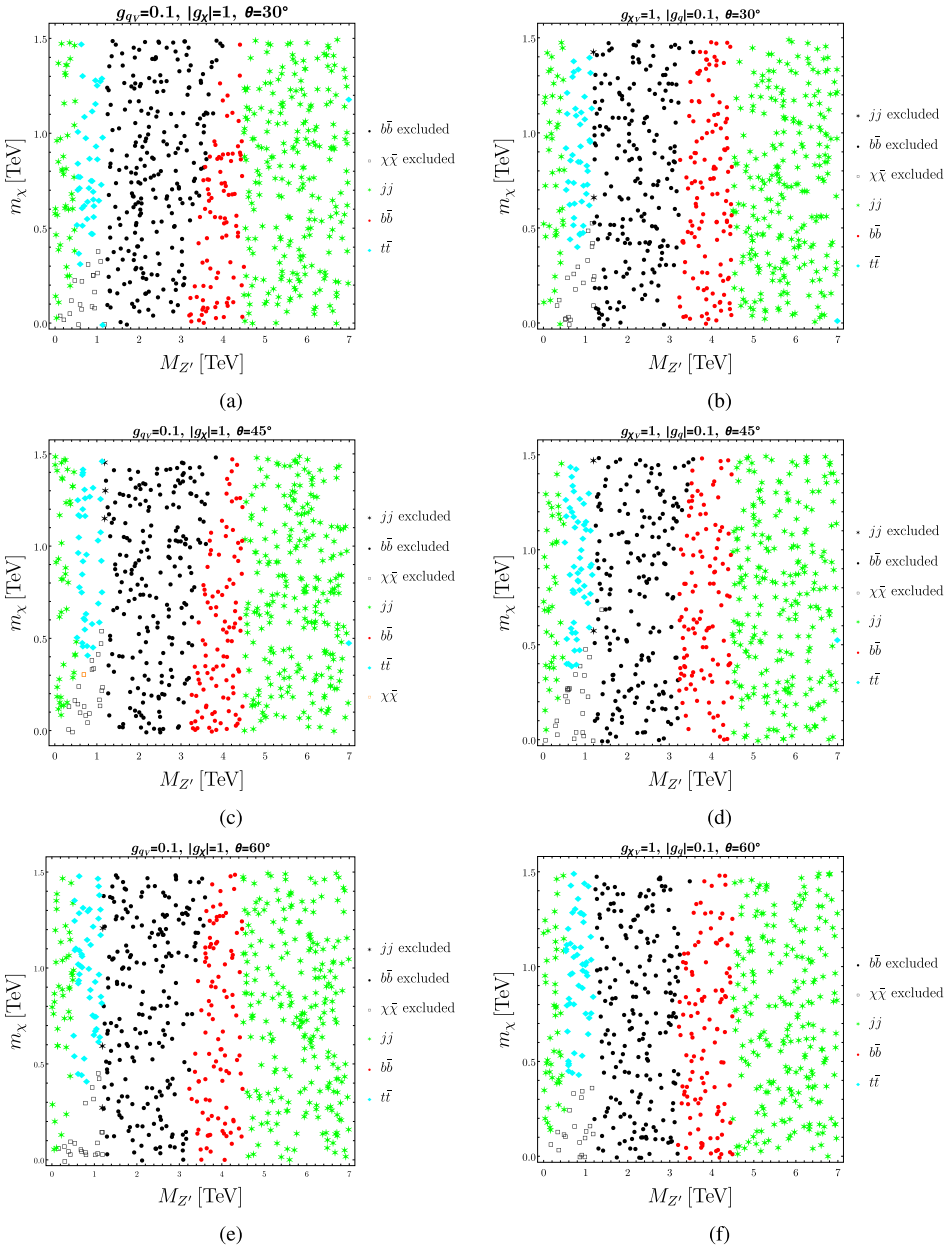

Fig. 8. Excluded parameter space and most sensitive channel for the case where the SM quarks couple with both vector and axial-vector couplings (left column of plots) and where the dark matter couples with both vector and axial-vector couplings (right column), fixing $g_{qV} = 0.1$ and $|g_\chi| = 1$. The upper, middle and lower panels show the case where the phase θ between the vector and axial-vector case are 30°, 45° and 60°, respectively.

According to Table 3 this charge combination remains massless before electroweak symmetry breaking. The other three $U(1)$ gauge bosons left acquire masses by the Stückelberg mechanism [61,62]. Here, we will assume that only one of these bosons is light enough to produce interesting phenomenology at collider energies while the other two are heavy enough to be decoupled from any effect. So any matter field ψ_α will couple to the lightest Z' boson as a combination of the different charges to the $U(1)$ factors,

$$g_\alpha^{Z'} = aQ_{\alpha A} + bQ_{\alpha B} + cQ_{\alpha C} + dQ_{\alpha D} + \sum_{i=1}^{m} h_i Q_{\alpha i}^h, \tag{6}$$

where h_i are the couplings to the hidden sector. Once we know how the Z' couples to matter and also the information of the charge assignment given in Table 3 we can derive the actual couplings of the SM particles to the Z'. As we mentioned before the quark sector is divided between the first and second generation and the third one, as they are charged differently they will consequently have different couplings. The couplings for the first and second generation of quarks are,

$$g_L^{u,c,d,s} = (a+b), \quad g_R^{u,c} = (-a+c), \quad g_R^{d,s} = (-a-c). \tag{7}$$

The couplings for the top and bottom quarks read,

$$g_L^{t,b} = (a-b), \quad g_R^{t} = (-a+c), \quad g_R^{b} = (-a-c). \tag{8}$$

Table 4
Different values of the couplings for the three phenomenological scenarios to be tested against Z'-explorer 2.0.

Scenario	a	b	c	d	g_χ^L	g_χ^R
1	0.07	0.00058	0.01	0.006	1.0	-1.0
2	-0.025	-0.005	0.005	0.025	1.0	1.0
3	0.1	-0.01	0.01	0.01	1.0	1.0

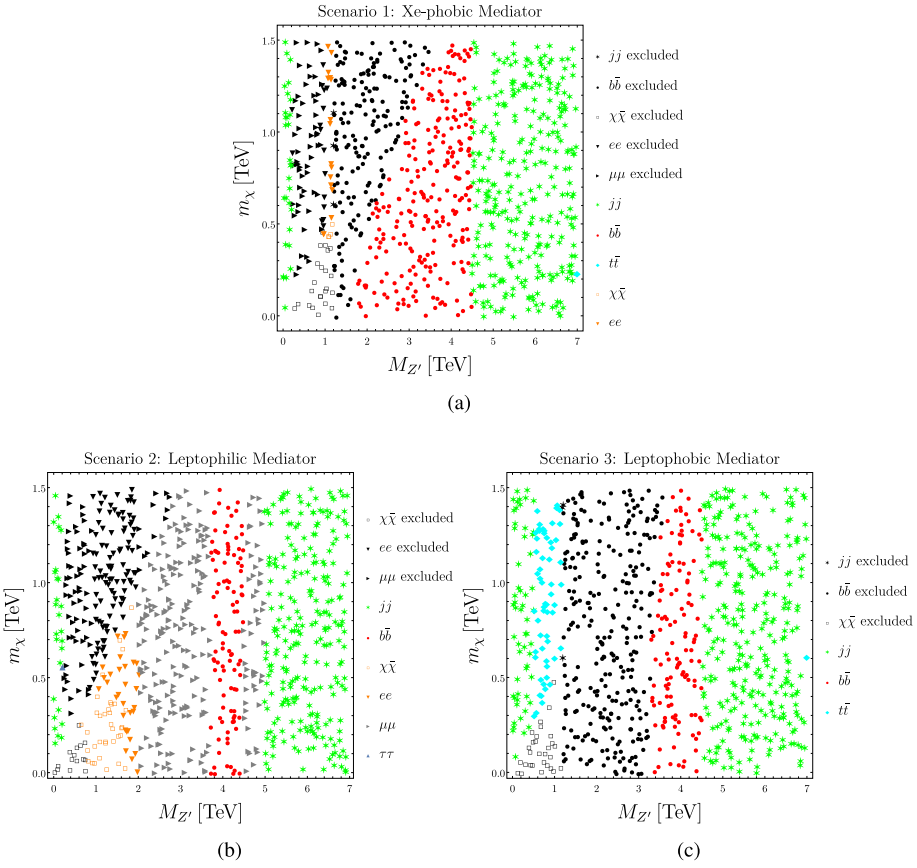

Fig. 9. Excluded parameter space and most sensitive channel for the case of the scenarios listed in Table 4.

And finally the couplings to the leptons are,

$$g_L^{\ell,\nu} = (-b-d), \quad g_R^{\ell} = (-c+d). \tag{9}$$

As we can see in the lepton sector there are no distinctions among families. For the sake of simplicity, we will consider that the dark matter couples to the Z' boson with two different couplings representing the left and right ones, g_χ^L and g_χ^R.

One of the aspects that makes this kind of portal attractive to explain the dark matter sector is the fact that the SM couplings to the Z' can be quite general. In that way, the dark matter particle will couple differently through the Z' to protons and neutrons, since the up and down couplings are different. Thus, this will be translated to non-zero isospin violation, f_n/f_p, as the general case. This affects directly to the phenomenology of dark matter since the dark matter direct detection experiments rely on the particle dark matter scattering off nuclei [63].

Once we have set the model and obtained the couplings we can now test it against Z'-explorer. In order to scrutinize the parameter space of the model we have chosen different scenarios that are phenomenologically interesting, they are shown in Table 4.

First of all, we examine Scenario 1 where we have an amount of isospin violation that makes Xenon-based direct detection of dark matter experiments less sensitive to the Z'. This kind of scenario is usually called Xe-phobic. The amount of isospin violation that one needs to obtain this is $f_n/f_p = -0.7$, so in our construction, this is achieved by a combination of the left and right parameters such as $b/c \simeq 0.0588$.[12] The parameters that define this scenario are listed in Table 4 while we scan the mass of the dark matter particle and the Z' in the ranges $m_\chi \in (0-1.5)$ TeV and $m_\chi \in (0-8)$ TeV. The results are depicted in the top plot of Fig. 9.

The results for Scenario 1 show the versatility in searches performed by Z'-explorer. First of all, we can see that for low dark matter masses and when this decay channel is kinematically allowed the monojet search can exclude up to dark matter masses of $m_\chi \sim 400$ GeV for masses of the Z' up to 1.1 TeV. In the same mass region of the Z' but for larger masses of the dark matter that closes the

[12] Details on how the amount of isospin violation is related with the parameters of the model can be found in Ref. [60].

$Z' \to \chi\chi$ channel, the leptonic searches are the most sensitive ones. The electron and muon searches can exclude all the region between $M_{Z'} = (0.4 - 1.1)$ TeV. While the exclusion for larger masses of Z' is due to the b-quark searches.

In the second scenario, we have chosen the parameters to decrease the b-quark coupling with respect to the previous scenario. This allows the coupling to leptons to be predominant and that is the reason why we call this scenario leptophilic even if there are some parts of the parameter region where the decay to quarks (including the b-quark) can be significant. The monojet channel is the most sensitive one for Z' masses up to 1.6 TeV when the dark matter decay channel is open. However, the power of exclusion only reaches until $M_{Z'}$=1 TeV. When the dark matter channel is not kinematically allowed the electron and muon searches can cover the mass range of $M_{Z'} = (400 - 2000)$ GeV. One then can find different most sensitive channels for the rest of the parameter space. However, the tiny values of the couplings and the large mass of the Z' make the total cross-section small enough so it lies under the reach of the experimental searches.

The third and last scenario corresponds to the opposite of Scenario 2. In this case, the values of the parameters are chosen in such a way that the vector and axial couplings of the leptons to the Z' vanish. This can be seen in the results of the right plot in Fig. 9. The most sensitive channels in all the parameter space are the monojet, $b\bar{b}$, $t\bar{t}$ and dijet. The monojet region here is very clear. When the dark matter decay channel is kinematically open the monojet search excludes up to masses of $M_{Z'}$. In this mass range but for a non-kinematically allowed dark matter channel the two most sensitive channels are $t\bar{t}$ and dijet, but they are not powerful enough to exclude. In the range of masses between $M_{Z'} = (1 - 4.5)$ TeV the $b\bar{b}$ search is the most sensitive allowing us to exclude masses that are lower than $M_{Z'} \lesssim 3.2$ TeV.

5. Conclusions

In this work, we have presented the expansion of the code Z'-explorer to further include missing energy searches, where Z' plays the role of a mediator between the dark and visible sectors. We have implemented within the existing Z'-explorer framework, which already included all LHC searches for Z' bosons with masses above the weak scale, the ATLAS mono-jet study with 139 fb^{-1} of data. We have found a good agreement between our simulations and the ATLAS results, which allowed us to make an exploratory journey of several Z' models.

In passing, we also commented on the difficulties encountered in the reinterpretation of the mono-jet study given the available reinterpretation material. While we had indeed found a good agreement, the material at our disposal was not always sufficient. For instance, we have benefited from the fact that two different versions of this study used each a different single benchmark point. Only having had one benchmark, the validation of the study would have lacked robustness. We would have also benefited from having access to the 95% C.L. upper limits instead of only having the 95% C.L. exclusion contours, and it would have been desirable that both exclusive and inclusive selections results were presented for the upper limits and exclusion contours.

We have studied the non-trivial interplay between the visible and invisible channels for dark matter and showed how they depend on the different coupling choices. In the first step, we have to take a bottom-up approach, considering the different Z' couplings as free, independent parameters. We have departed from the simplifying assumptions of universal couplings for quarks and leptons, showing the rich palette of phenomenological possibilities. We have also explored the impact of the dark matter coupling neither vectorially nor axially to the dark matter particle, showing that even for a non-trivial configuration that involves more channels Z' arises as a powerful tool to test the different regions of the parameter space. These excursions in the simplified model space highlight the importance of having a broad program of experimental searches, as no single channel dominates over the whole parameter space.

However, in explicit Z' models which derive from top-down considerations, there often exist correlations among the different couplings. We have then considered a Stückelberg portal that is obtained as low energy effective actions in some string compactifications with intersecting branes in type IIa string theory. In this construction the Z' couples to the matter fields via a combination of four different charges. Consequently, the parameter space is more complex, involving more parameters and correlations between couplings. With the aid of Z'-explorer 2.0, we have derived the exclusion limits in the $M_{Z'} - m_\chi$ plane for different benchmark scenarios. Even for a more complex coupling construction, Z'-explorer is to be a powerful tool. While different parameter choices in the Stückelberg portal seem to prefer different visible channels, the mono-jet channel added in this version appears ubiquitously in the three scenarios explored. This specific search then has a crucial role in testing models that have Z' when the dark matter channel is open.

Along the way, we have also highlighted the potential improvements that could be added to the code, for example, the addition of flavor bounds, considering Z' in the GeV range (known as *dark photons* in the jargon, they are well covered by DarkCast [64]), extrapolating the results to the High-Luminosity LHC (HL-LHC and future colliders), or enlarging the particle content of the dark sector. We leave these interesting options, among others, as possible avenues for improvement for a new version.

Declaration of competing interest

The authors declare that they have no known competing financial interests or personal relationships that could have appeared to influence the work reported in this paper.

Data availability

The code is publicly available on Github, and is linked on the publication.

Acknowledgements

We would like to thank Ezequiel Alvarez for his collaboration in the early stages of this work. We are indebted to Benjamin Fuks and Dipan Sengupta for correspondence regarding the MadAnalysis5 PAD implementation of reference [65] and to Boyu Gao for useful cross-checks of the event generation setup. We would also like to thank Giuliano Gustavino, Valerio Ippolito and Steven Worm for useful communication regarding technical details of the ATLAS analysis, and Marie-Hélène Genest and Nishita Desai for useful discussions. We

also thank Diego Mouriño for assistance with the code. JZ is supported by the *Generalitat Valenciana* (Spain) through the *plan GenT* program (CIDEGENT/2019/068). VML is funded by the Deutsche Forschungsgemeinschaft (DFG, German Research Foundation) under Germany's Excellence Strategy - EXC 2121 "Quantum Universe" - 39083330. We also want to thank the organizers of the "(Re)interpreting the results of new physics searches at the LHC" and "Río de la Plata Ph-Exp Institute" workshops and the IFLP where the starting point of this project took off.

Appendix A. Z'-explorer 2.0: implementation details

A.1. Backend

As previously described, Z'-explorer 2.0 extend the scope of the software's first version to include final states with missing transverse energy. The implementation for the SM (*visible*) channels remains unchanged, see [12] for further details. In this version we have modified some of the visible channels to include the most sensitive searches up to date. The updated references for each visible channel are: jj [46], $b\bar{b}$ [46], $t\bar{t}$ [47], e^+e^- [48], $\mu^+\mu^-$ [48], $\tau^+\tau^-$ [49], W^+W^- [50], Zh [51]. Therefore, in this appendix we focus on the implementation of the new DM final state.

To compute the production cross section in the new decay channel, the software uses previously generated and recorded the leading order (LO) $pp \to Z'j$ cross section (instead of just $q\bar{q} \to Z'$, used for visible channels) at $\sqrt{s} = 13$ TeV with `MadGraph5_aMC@NLO`, customizing the UFO-model described in section 2, to set $g_{q_A} = g_{q_V} = 1$ for only one quark in the proton each time, for $M_{Z'} \in [0.01, 2, 5]$ TeV, with a step of 0.01 TeV. We have explicitly verified that the initial states with b quarks have a negligible contribution to this process. We employ default settings of `MadGraph5_aMC@NLO`, and in particular the fast detector simulation uses the ATLAS default card from `Delphes 3.4.2`.

These cross sections grids, stored in the repository as `/cards/AXIAL(VEC)_Zpj`, are invoked during the program execution: the predicted production cross section for a benchmark point is simply the sum of the four contributions of quarks (u, d, c and s), each of them adjusted by the sum of the corresponding squared couplings. That is

$$\sigma(pp \to Z'j)^{g_{q_A},\, g_{q_V}} = \sum_q \left[\sigma(pp \to Z'j)^{g_{q_A}=1}(g_{q_A})^2 + \sigma(pp \to Z'j)^{g_{q_V}=1}(g_{q_V})^2\right] \tag{A.1}$$

The software selects inside the simulations the record with the mass $M_{Z'}$ that is closest to the one in the input card at the corresponding benchmark point.[13] The axial and vector couplings are directly estimated from the chiral coupling in the input card ("incard")

$$g_{f_V} = \frac{1}{2}(g_{f_R} + g_{f_L}), \qquad g_{f_A} = \frac{1}{2}(g_{f_R} - g_{f_L}). \tag{A.2}$$

The production cross-section times branching ratio ($\mathcal{BR}(Z' \to \chi\bar{\chi})$) is finally estimated within the NWA for the given benchmark point, and is used to re-scale the experimental limits in [17] for the axial-vector mediator scenario.[14] The number of events in each exclusive signal region (coming from our recast previously described) are stored for the set of points in the $(M_{Z'}, m_\chi)$ plane mentioned in section 3, in different text files in `/cards/DM/AXIAL` folder, which were obtained under the hypothesis of $g_q = 0.25$ and $g_\chi = 1$. The software selects the file for the $(M_{Z'}, m_\chi)$ pair that is closest to the one in the input card at the corresponding benchmark point, through the determination of the euclidean norm. As mentioned in the main text, this is the main difference concerning the first version: having upper limits and exclusion contours in 2 dimensions instead of only one. The signal events are re-scaled by multiplying by the ratio between the aforementioned production cross-section times branching ratio for the required (g_q, g_χ) values, and the production cross-section times branching ratio estimated for the benchmark point used by ATLAS, with reference values of $(0.25, 1)$. With the corresponding events selected and properly re-scaled as explained, the software selects the most sensitive EM signal region compared to background (also stored in `/cards/DM/`) and estimates the strength for the $\chi\bar{\chi}$ channel.

A.2. Frontend

The input card (`/incard/card_1.dat`) required in Z'-explorer 2.0 is quite similar to the one needed in its first version. The user must provide the old requirements for the visible channels: $M_{Z'}$ (in TeV), the Z' couplings to all SM-fermions, except for neutrinos, which information is required through the partial width $\Gamma_{\nu\nu}$, as for the W^+W^- (Γ_{WW}) and the Zh (Γ_{Zh}) decay channels. These entries are required as *partial width* since there is not a unique Lorentz structure in their couplings. Additionally, for the new channel, we require the fermionic DM mass m_χ (in TeV), and its couplings to Z'. The total width to other non-SM particles can be added in the computation as Γ_{xx}. Each entry is one row (with twenty-six columns), and corresponds to one benchmark point within the model to be tested by Z'-explorer 2.0. The NP parameters should be specified in the following order (with each column separated by spaces)

$$M_{Z'}\ g_{u_L}\ g_{u_R}\ g_{d_L}\ g_{d_R}\ g_{c_L}\ g_{c_R}\ g_{s_L}\ g_{s_R}\ g_{b_L}\ g_{b_R}\ g_{t_L}\ g_{t_R}\ g_{e_L}\ g_{e_R}\ g_{\mu_L}\ g_{\mu_R}\ g_{\tau_L}\ g_{\tau_R}\ \Gamma_{\nu\nu}\ \Gamma_{WW}\ \Gamma_{Zh}\ m_\chi\ g_{\chi_L}\ g_{\chi_R}\ \Gamma_{xx} \tag{A.3}$$

where g_{f_L} (g_{f_R}) is the coupling of Z' to the corresponding Left (Right) fermion. To obtain the right form of the $g_{f_{L/R}}$ couplings from a given NP model, interactions between Z' and SM fermions must be written in the parametrization of equation (1).

The instruction for running the software remains unchanged. In the command line type

```
>./program.out
```

[13] Our algorithm has proven to be more accurate than a 2-D interpolation in the $M_{Z'} - m_\chi$ plane.

[14] The case for the vector mediator can be trivially derived from the axial one, so we will describe the latter only, for simplicity.

The software displays on the command shell a summary of the tasks performed during execution. The addition of the new invisible channel does not significantly change the speed of the performance from the first version ($\mathcal{O}(10^3)$ points can be processed in no more than 2 seconds in a regular CPU).Z'-explorer 2.0 prints in the output file (`/output/1.dat`) the incard information for each benchmark point (to ease the after-processing), followed by

$$\mathcal{S}_{jj} \quad \mathcal{S}_{bb} \quad \mathcal{S}_{tt} \quad \mathcal{S}_{ee} \quad \mathcal{S}_{\mu\mu} \quad \mathcal{S}_{\tau\tau} \quad \mathcal{S}_{\nu\nu} \quad \mathcal{S}_{WW} \quad \mathcal{S}_{Zh} \quad \mathcal{S}_{\chi\chi} \quad \mathcal{S}_{xx} \quad \Gamma_{Z'} \quad WARNING : \Gamma_{Z'} > 5 \tag{A.4}$$

where $\mathcal{S}$ is the calculated strength in each channel (already defined in [12]), $\Gamma_{Z'}$ is the Z' total width, and the last column is a warning for when the input parameters invalidate the narrow width approximation (displays 1 if $\Gamma_{Z'} > 5\%$ and 0 otherwise). Nonetheless, this warning does not halt the execution, so the resulting rate is computed using NWA even if it is not a good approximation. The parameter $\mathcal{S}_{xx}$ can be regarded as a dummy variable to eventually add experimental information of other possible non-SM Z' channels. For further details about running and the additional information that can be extracted from Z'-explorer 2.0, visit the GitHub repository [21].

References

[1] W. Abdallah, et al., SciPost Phys. 9 (2) (2020) 022, https://doi.org/10.21468/SciPostPhys.9.2.022, arXiv:2003.07868.
[2] M. Drees, H. Dreiner, D. Schmeier, J. Tattersall, J.S. Kim, Comput. Phys. Commun. 187 (2015) 227–265, https://doi.org/10.1016/j.cpc.2014.10.018, arXiv:1312.2591.
[3] D. Dercks, N. Desai, J.S. Kim, K. Rolbiecki, J. Tattersall, T. Weber, Comput. Phys. Commun. 221 (2017) 383–418, https://doi.org/10.1016/j.cpc.2017.08.021, arXiv:1611.09856.
[4] B. Dumont, B. Fuks, S. Kraml, S. Bein, G. Chalons, E. Conte, S. Kulkarni, D. Sengupta, C. Wymant, Eur. Phys. J. C 75 (2) (2015) 56, https://doi.org/10.1140/epjc/s10052-014-3242-3, arXiv:1407.3278.
[5] E. Conte, B. Fuks, Int. J. Mod. Phys. A 33 (28) (2018) 1830027, https://doi.org/10.1142/S0217751X18300272, arXiv:1808.00480.
[6] P. Athron, et al., Eur. Phys. J. C 77 (11) (2017) 784; Addendum: Eur. Phys. J. C 78 (2018) 98, https://doi.org/10.1140/epjc/s10052-017-5321-8, arXiv:1705.07908.
[7] P. Bechtle, D. Dercks, S. Heinemeyer, T. Klingl, T. Stefaniak, G. Weiglein, J. Wittbrodt, Eur. Phys. J. C 80 (12) (2020) 1211, https://doi.org/10.1140/epjc/s10052-020-08557-9, arXiv:2006.06007.
[8] H. Bahl, V.M. Lozano, T. Stefaniak, J. Wittbrodt, Testing exotic scalars with HiggsBounds, 9 2021, arXiv:2109.10366.
[9] P. Bechtle, S. Heinemeyer, T. Klingl, T. Stefaniak, G. Weiglein, J. Wittbrodt, Eur. Phys. J. C 81 (2) (2021) 145, https://doi.org/10.1140/epjc/s10052-021-08942-y, arXiv:2012.09197.
[10] S. Kraml, S. Kulkarni, U. Laa, A. Lessa, W. Magerl, D. Proschofsky-Spindler, W. Waltenberger, Eur. Phys. J. C 74 (2014) 2868, https://doi.org/10.1140/epjc/s10052-014-2868-5, arXiv:1312.4175.
[11] M. Papucci, K. Sakurai, A. Weiler, L. Zeune, Eur. Phys. J. C 74 (11) (2014) 3163, https://doi.org/10.1140/epjc/s10052-014-3163-1, arXiv:1402.0492.
[12] E. Alvarez, M. Estévez, R.M. Sandá, Comput. Phys. Commun. 269 (2021) 108144, https://doi.org/10.1016/j.cpc.2021.108144, arXiv:2005.05194.
[13] A. Leike, Phys. Rep. 317 (1999) 143–250, https://doi.org/10.1016/S0370-1573(98)00133-1, arXiv:hep-ph/9805494.
[14] P. Langacker, Rev. Mod. Phys. 81 (2009) 1199–1228, https://doi.org/10.1103/RevModPhys.81.1199, arXiv:0801.1345.
[15] O. Buchmueller, M.J. Dolan, S.A. Malik, C. McCabe, J. High Energy Phys. 01 (2015) 037, https://doi.org/10.1007/JHEP01(2015)037, arXiv:1407.8257.
[16] D. Abercrombie, et al., Phys. Dark Universe 27 (2020) 100371, https://doi.org/10.1016/j.dark.2019.100371, arXiv:1507.00966.
[17] G. Aad, et al., Phys. Rev. D 103 (11) (2021) 112006, https://doi.org/10.1103/PhysRevD.103.112006, arXiv:2102.10874.
[18] E. Bernreuther, J. Horak, T. Plehn, A. Butter, SciPost Phys. 5 (4) (2018) 034, https://doi.org/10.21468/SciPostPhys.5.4.034, arXiv:1805.11637.
[19] F. Kahlhoefer, A. Mück, S. Schulte, P. Tunney, J. High Energy Phys. 03 (2020) 104, https://doi.org/10.1007/JHEP03(2020)104, arXiv:1912.06374.
[20] D.M. Straub, flavio: a Python package for flavour and precision phenomenology in the Standard Model and beyond, 10 2018, arXiv:1810.08132.
[21] V.M. Lozano, R.M. Sandá Seoane, J. Zurita, Source scripts for software in this work, GIT repository, https://github.com/ro-sanda/Z--explorer-2.0.
[22] F. Kahlhoefer, K. Schmidt-Hoberg, T. Schwetz, S. Vogl, J. High Energy Phys. 02 (2016) 016, https://doi.org/10.1007/JHEP02(2016)016, arXiv:1510.02110.
[23] Y. Cui, F. D'Eramo, Phys. Rev. D 96 (9) (2017) 095006, https://doi.org/10.1103/PhysRevD.96.095006, arXiv:1705.03897.
[24] C. Degrande, C. Duhr, B. Fuks, D. Grellscheid, O. Mattelaer, T. Reiter, Comput. Phys. Commun. 183 (2012) 1201–1214, https://doi.org/10.1016/j.cpc.2012.01.022, arXiv:1108.2040.
[25] http://feynrules.irmp.ucl.ac.be/wiki/DMsimp.
[26] J. Alwall, R. Frederix, S. Frixione, V. Hirschi, F. Maltoni, O. Mattelaer, H.S. Shao, T. Stelzer, P. Torrielli, M. Zaro, J. High Energy Phys. 07 (2014) 079, https://doi.org/10.1007/JHEP07(2014)079, arXiv:1405.0301.
[27] T. Sjöstrand, S. Ask, J.R. Christiansen, R. Corke, N. Desai, P. Ilten, S. Mrenna, S. Prestel, C.O. Rasmussen, P.Z. Skands, Comput. Phys. Commun. 191 (2015) 159, https://doi.org/10.1016/j.cpc.2015.01.024, arXiv:1410.3012.
[28] J. de Favereau, C. Delaere, P. Demin, A. Giammanco, V. Lemaître, A. Mertens, M. Selvaggi, J. High Energy Phys. 02 (2014) 057, https://doi.org/10.1007/JHEP02(2014)057, arXiv:1307.6346.
[29] M. Backović, M. Krämer, F. Maltoni, A. Martini, K. Mawatari, M. Pellen, Eur. Phys. J. C 75 (10) (2015) 482, https://doi.org/10.1140/epjc/s10052-015-3700-6, arXiv:1508.05327.
[30] J. Alwall, C. Duhr, B. Fuks, O. Mattelaer, D.G. Öztürk, C.-H. Shen, Comput. Phys. Commun. 197 (2015) 312–323, https://doi.org/10.1016/j.cpc.2015.08.031, arXiv:1402.1178.
[31] G. Bélanger, F. Boudjema, A. Goudelis, A. Pukhov, B. Zaldivar, Comput. Phys. Commun. 231 (2018) 173–186, https://doi.org/10.1016/j.cpc.2018.04.027, arXiv:1801.03509.
[32] C. Arina, J. Heisig, F. Maltoni, D. Massaro, O. Mattelaer, Indirect dark-matter detection with MadDM v3.2 – lines and loops, 7 2021, arXiv:2107.04598.
[33] Dark matter summary plots for s-channel, 2HDM+a and Dark Higgs models, Tech. Rep., CERN, Geneva, 2022, all figures including auxiliary figures are available at https://atlas.web.cern.ch/Atlas/GROUPS/PHYSICS/PUBNOTES/ATL-PHYS-PUB-2022-036, http://cds.cern.ch/record/2816368.
[34] G. Aad, et al., Search for dark matter produced in association with a Standard Model Higgs boson decaying into b-quarks using the full Run 2 dataset from the ATLAS detector, 8 2021, arXiv:2108.13391.
[35] M. Aaboud, et al., J. High Energy Phys. 10 (2018) 180, https://doi.org/10.1007/JHEP10(2018)180, arXiv:1807.11471.
[36] M. Aaboud, et al., Phys. Lett. B 776 (2018) 318–337, https://doi.org/10.1016/j.physletb.2017.11.049, arXiv:1708.09624.
[37] G. Aad, et al., J. High Energy Phys. 02 (2021) 226, https://doi.org/10.1007/JHEP02(2021)226, arXiv:2011.05259.
[38] A. Tumasyan, et al., Search for new particles in events with energetic jets and large missing transverse momentum in proton-proton collisions at $\sqrt{s} = 13$ TeV, 7 2021, arXiv:2107.13021.
[39] A.M. Sirunyan, et al., Phys. Rev. D 97 (9) (2018) 092005, https://doi.org/10.1103/PhysRevD.97.092005, arXiv:1712.02345.
[40] A.M. Sirunyan, et al., J. High Energy Phys. 07 (2017) 014, https://doi.org/10.1007/JHEP07(2017)014, arXiv:1703.01651.
[41] A.M. Sirunyan, et al., J. High Energy Phys. 10 (2017) 073, https://doi.org/10.1007/JHEP10(2017)073, arXiv:1706.03794.
[42] M. Aaboud, et al., J. High Energy Phys. 01 (2018) 126, https://doi.org/10.1007/JHEP01(2018)126, arXiv:1711.03301.
[43] D. Sengupta, Implementation of a search for dark matter in the mono-jet channel (36.1 fb-1; 13 TeV; ATLAS-EXOT-2016-27), https://doi.org/10.14428/DVN/DFQPGU, 2021.
[44] M. Aaboud, et al., Phys. Rev. D 96 (7) (2017) 072002, https://doi.org/10.1103/PhysRevD.96.072002, arXiv:1703.09665.
[45] V. Khachatryan, et al., J. Instrum. 12 (02) (2017) P02014, https://doi.org/10.1088/1748-0221/12/02/P02014, arXiv:1607.03663.
[46] G. Aad, et al., Search for new resonances in mass distributions of jet pairs using 139 fb^{-1} of pp collisions at $\sqrt{s} = 13$ TeV with the ATLAS detector, arXiv:1910.08447, 2019.
[47] A.M. Sirunyan, et al., J. High Energy Phys. 04 (2019) 031, https://doi.org/10.1007/JHEP04(2019)031, arXiv:1810.05905.
[48] A.M. Sirunyan, et al., J. High Energy Phys. 07 (2021) 208, https://doi.org/10.1007/JHEP07(2021)208, arXiv:2103.02708.
[49] M. Aaboud, et al., J. High Energy Phys. 01 (2018) 055, https://doi.org/10.1007/JHEP01(2018)055, arXiv:1709.07242.

[50] A. Tumasyan, et al., Search for heavy resonances decaying to WW, WZ, or WH boson pairs in the lepton plus merged jet final state in proton-proton collisions at $\sqrt{s}$ = 13 TeV, 9 2021, arXiv:2109.06055.
[51] A.M. Sirunyan, et al., Phys. Lett. B 798 (2019) 134952, https://doi.org/10.1016/j.physletb.2019.134952, arXiv:1906.00057.
[52] C. Shimmin, D. Whiteson, Phys. Rev. D 94 (5) (2016) 055001, https://doi.org/10.1103/PhysRevD.94.055001, arXiv:1602.07727.
[53] A.M. Sirunyan, et al., J. High Energy Phys. 01 (2018) 097, https://doi.org/10.1007/JHEP01(2018)097, arXiv:1710.00159.
[54] M. Aaboud, et al., Phys. Lett. B 788 (2019) 316–335, https://doi.org/10.1016/j.physletb.2018.09.062, arXiv:1801.08769.
[55] P. Langacker, R.W. Robinett, J.L. Rosner, Phys. Rev. D 30 (1984) 1470, https://doi.org/10.1103/PhysRevD.30.1470.
[56] F. Del Aguila, M. Cvetic, Phys. Rev. D 50 (1994) 3158–3166, https://doi.org/10.1103/PhysRevD.50.3158, arXiv:hep-ph/9312329.
[57] L.E. Ibanez, F. Marchesano, R. Rabadan, J. High Energy Phys. 11 (2001) 002, https://doi.org/10.1088/1126-6708/2001/11/002, arXiv:hep-th/0105155.
[58] W.-Z. Feng, G. Shiu, P. Soler, F. Ye, Phys. Rev. Lett. 113 (2014) 061802, https://doi.org/10.1103/PhysRevLett.113.061802, arXiv:1401.5880.
[59] W.-Z. Feng, G. Shiu, P. Soler, F. Ye, J. High Energy Phys. 05 (2014) 065, https://doi.org/10.1007/JHEP05(2014)065, arXiv:1401.5890.
[60] V.M. Lozano, M. Peiró, P. Soler, J. High Energy Phys. 04 (2015) 175, https://doi.org/10.1007/JHEP04(2015)175, arXiv:1503.01780.
[61] E.C.G. Stueckelberg, Helv. Phys. Acta 11 (1938) 225–244, https://doi.org/10.5169/seals-110852.
[62] E.C.G. Stueckelberg, Helv. Phys. Acta 11 (1938) 299–328.
[63] J.L. Feng, J. Kumar, D. Marfatia, D. Sanford, Phys. Lett. B 703 (2011) 124–127, https://doi.org/10.1016/j.physletb.2011.07.083, arXiv:1102.4331.
[64] P. Ilten, Y. Soreq, M. Williams, W. Xue, J. High Energy Phys. 06 (2018) 004, https://doi.org/10.1007/JHEP06(2018)004, arXiv:1801.04847.
[65] M. Aaboud, et al., J. High Energy Phys. 01 (2018) 126, https://doi.org/10.1007/JHEP01(2018)126, arXiv:1711.03301.